Conference on Modelling Fluid Flow (CMFF'25)
The 19th International Conference on Fluid Flow Technologies
Budapest, Hungary, August 26 - August 29, 2025

INVESTIGATING THE INFLUENCE OF PARTICLE SHAPE ON THE PYROLYSIS OF THERMALLY THICK PARTICLES IN DEM/CFD

Bo JAEGER[1,2], Rezvan ABDI[2], Enric ILLANA[2], Viktor SCHERER[2]

[1] Corresponding Author. Tel.: +49 234 32 23503. E-Mail: jaeger@leat.rub.de
[2] Institute of Energy Plant Technology, Ruhr-University Bochum, Universitätsstraße 150, 44780 Bochum, Germany.

ABSTRACT

Understanding how particle shape and packing arrangement affect heat transfer and flow dynamics is essential for accurately modeling pyrolysis in fixed particle beds. This study investigates the influence of particle geometry and bed structure on pyrolysis behavior, focusing on spherical, cylindrical, and cubical particles. As numerical tool, the coupling of Computational Fluid Dynamics (CFD) with the Discrete Element Method (DEM) is used incorporating a radiation model based on the Discrete Ordinates Method (DOM).

The results reveal that particle shape and spatial particle arrangement significantly influence local flow patterns, temperature gradients, and pyrolysis progression. While packings of spherical particles exhibit more uniform heating, beds of cylindrical and cubical particles demonstrate complex interactions between radiation and convection due to geometric shadowing of radiation and directional flow channels. In total, the pyrolysis progess of the bed is fastest for spheres, followed by cylinders and cubes.

Keywords: Blocked-Off, DEM/CFD, Particle shape, Pyrolysis

NOMENCLATURE

A	[m^2]	surface area
D_i	[m^2 s^{-1}]	diffusion coefficient
E	[W m^3 sr^{-1}]	emission
$\underline{F_i}$	[N]	force
I	[W m^3 sr^{-1}]	radiative intensity
$\underline{J}$	[kg m^2]	inertia of the body
$\underline{L}$	[kg m^2 s^{-1}]	angular momentum
$\underline{M_j}$	[Nm]	torque
N_i	[-]	number of i
$\underline{P}$	[kg m s^{-1}]	translational momentum
$\underline{s}$	[-]	radiation direction vector
S_E	[J m^{-3} s^{-1}]	enthalpy source term
S_{gas}	[kg m^{-3} s^{-1}]	mass source
S_i	[kg m^{-3}s^{-1}]	mass source of species i
S_M	[kg m^{-2} s^{-2}]	momentum source
T	[K]	temperature
Y_i	[-]	mass fraction
$\underline{g}$	[m s^{-2}]	gravitational acceleration
h_f	[J kg^{-1}]	specific enthalpy
k_f	[Wm^{-1} K^{-1}]	thermal conductivity
p_{rgh}	[N m^{-2}]	gauge pressure
$\underline{r_i}$	[m]	position vector
t	[s]	time
$\underline{u_f}$	[m s^{-1}]	velocity
$\underline{x}$	[m]	particle / cell position
ε	[-]	bed porosity
ρ_f	[kg m^{-3}]	density
τ_f	[Pa]	stress tensor
φ	[-]	surface area ratio
$\underline{\omega}$	[rad s^{-1}]	angular velocity

Subscripts and Superscripts

CV	control volume
f	fluid
p	particle
pf	particle face
$surf$	surface

1. INTRODUCTION

Pyrolysis is a thermochemical decomposition process in which organic materials are heated in the absence of oxygen, typically within a temperature range of 300 °C to 900 °C. This process is widely used in bioenergy applications, where it is a precursor step to combustion or where it enables the conversion of solid biomass into valuable fuels.

Although pyrolysis is a well-established process, achieving optimal efficiency and uniformity in fixed-bed pyrolysis reactors remains a significant challenge. The local arrangement of particles within the bed and their shape strongly influences flow fields, heat transfer, and ultimately, the rate and uniformity of thermal conversion. This paper aims to provide insight into this complex problem.

Copyright© Department of Fluid Mechanics, Budapest University of Technology and Economics and the Authors

Pyrolysis of fixed beds of solid particles in DEM/CFD was already in the focus of previous studies. For example, Mahmoudi et al. simulated the pyrolysis of spherical particles in a small-scale packed bed [1]. The same reactor was also modeled by Gao et al. but with cubical particles instead of spheres [2]. Other authors combined the pyrolysis with a subsequent combustion process. Wiese et al. used DEM/CFD to model the pyrolysis (and combustion) of cylindrical particles [3] in a domestic pellet stove. Buss et al. [4] investigated the thermal conversion of (agitated) beds of straw pellet, representing the particles as sphero-cylinder.

However, these studies were restricted to only a single particle shape. Hence, the influence of particle shape and the corresponding bed morphology on the pyrolysis process could not be investigated.

To study the influence of particle shape in pyrolysis a numerical method is required that captures the details of the flow field in the void spaces among particles. In DEM/CFD this is typically realized by Immersed Boundary Methods (IBM) [5]. Boundaries of solid objects (walls, particles) are numerically embedded into the CFD domain and the underlying system of fluid conservation equations and their presence in the fluid flow is accounted for without meshing the actual shape. IBMs were used by several groups to model the fluid flow through packings with [6,7] and without [8, 9] heat transfer.

A simple version of an IBM, the so called Blocked-Off approach (BO) [10, 11], is used in this work. All simulations shown are based on an inhouse DEM code coupled with the FireFOAM solver of OpenFOAM [12].

Special emphasis is placed on analysing three distinct particle geometries—spheres, cylinders, and cubes—to systematically investigate their influence on thermal gradients, inter-particle heat transfer, and local flow phenomena within the bed. Particular attention is paid to the spatially heterogeneous heating behaviour observed in packings of non-spherical particles, where complex radiation shadowing effects and orientation-dependent exposure to radiation and flow lead to significant variation in particle temperature and pyrolysis rate—even among neighbouring particles.

The structure of the article is organized as follows: Section 2 outlines the mathematical framework and the governing equations. Section 3 introduces and details the test scenarios, which include a pyrolysis reactor filled either with cubes, spheres, or cylinders. In Section 4, the results are analyzed and discussed in depth, while Section 5 provides a summary of the key findings.

2. NUMERICAL MODELS

The numerical model used in this study combines the DEM/CFD method with the "Blocked-Off" (BO) approach, a simplified form of the Immersed Boundary Method (IBM)

While we describe the BO in short in chapter 2.2.1–2.2.3, we refer to [8, 11, 13] for more details about the method used.

2.1 Particle mechanics (DEM)

The Discrete Element Method (DEM) was employed to generate the initial packed bed configuration. The dynamics of the particles are governed by the momentum equation for translation ($\underline{P}$) and rotation ($\underline{L}$). The translational acceleration of a particle center of gravity is calculated based on the total contact forces $\underline{F_i}$ and gravitational force $m\underline{g}$. (Eq. 1). The angular acceleration (Eq. 2) is obtained from the torque due to contact forces $\underline{F_i}$ (both normal and tangential):

$$\frac{d\underline{P}}{dt} = m \cdot \frac{d^2\underline{x}}{dt^2} = \sum_{i=1}^{n} \underline{F_i} + m\underline{g} \tag{1}$$

$$\begin{aligned} \frac{d\underline{L}}{dt} = \underline{\omega} \times \underline{J} \cdot \underline{\omega} + \underline{J} \cdot \underline{\dot{\omega}} = \sum_{i=1}^{n} \underline{M_i} \\ = \sum_{i=1}^{n} \underline{r_i} \times \underline{F_i} \end{aligned} \tag{2}$$

where $\underline{x}$ is the particle position, m is the mass, t represents time, $\underline{\omega}$ the angular velocity and $\underline{J}$ is the inertia of the body. Contact forces were calculated with a linear spring-dashpot model and particles were modelles as polyhedrons.

2.2 Computational Fluid Dynamics (CFD)

The CFD solver ensures conservation of mass (Eq. 3), momentum (Eq. 4), and energy (Eq. 5) within the fluid phase by solving the corresponding transport equations.

$$\frac{\partial \rho_f}{\partial t} + \underline{\nabla} \cdot \left(\rho_f \underline{u}_f\right) = S_{gas} \tag{3}$$

$$\begin{aligned} \frac{\partial (\rho_f \underline{u}_f)}{\partial t} + \underline{\nabla} \cdot \left(\rho_f \underline{u}_f \underline{u}_f\right) \\ = -\underline{\nabla} p_{rgh} + \underline{\nabla} \cdot \tau_f \\ + \underline{g}\underline{x} \cdot \underline{\nabla}\rho + \underline{S_M} \end{aligned} \tag{4}$$

$$\begin{aligned} \frac{\partial (\rho_f h_f)}{\partial t} + \underline{\nabla} \cdot \left(\rho_f \underline{u}_f h_f\right) \\ = \underline{\nabla} \cdot \left(k_f \, \underline{\nabla} T\right) + S_E \end{aligned} \tag{5}$$

The behavior of the fluid phase is defined through parameters such as specific enthalpy (h_f), velocity ($\underline{u}_f$), and density (ρ_f). The term S_{gas} represents the mass transfer between the fluid and solid phases. Sources contributing to momentum include the gauge pressure gradient ($\underline{\nabla} p_{rgh}$), stress

Copyright© Department of Fluid Mechanics, Budapest University of Technology and Economics and the Authors

tensor (τ_f) under the assumption of laminar flow, gravitational acceleration vector ($\underline{g}$) and momentum exchanged with the particles ($\underline{S_M}$). The vector field ($\underline{x}$) contains the cell centres.

In the context of energy transport, the fluid's ability to conduct heat is described by its thermal conductivity (k_f), and the enthalpy exchanged with the solid is expressed as S_E.

The transport equation for a chemical species i is expressed as:

$$\frac{\partial(\rho_f Y_\mathrm{i})}{\partial t} + \underline{\nabla}\cdot\left(\rho_f \underline{u}_f Y_\mathrm{i}\right) = \underline{\nabla}\cdot\left(\rho_f D_\mathrm{i}\,\underline{\nabla} Y_i\right) + S_\mathrm{i} \tag{6}$$

Where the source term S_i, and the term including the diffusion coefficient D_i, model the release and transport of i from the particles during the reaction, respectively.

2.2.1. Blocked-Off approach

The embedding of the particle surface within the CFD-domain is achieved by two means and is explained with Figure 1.: First, the CFD cells (CV) lying within the particle (core CV) and the cells containing the particle surface (surface CV) are determined. Cell faces belonging to both cell types are labeled as solid-fluid-interface. Scalar transport across these faces is turned off / blocked so that no fluid properties can penetrate the cell region occupied by a particle. Second, source terms S are calculated in the surface CVs and added to the fluid equations (Eqs. 3–5). The values of S depend on the local flow conditions and the properties of the discrete particle surface.

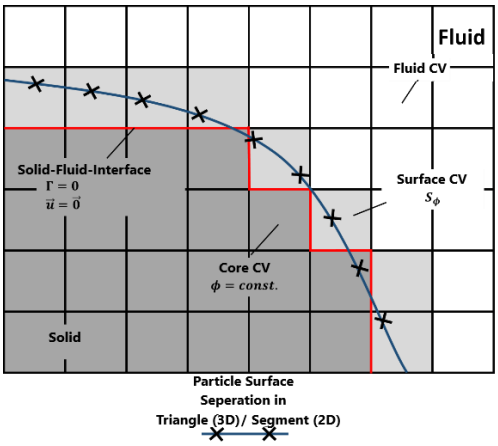

Figure 1. Schematic depiction of the BO-approach

By doing so, the fluid flow effectively evolves around the particle. The total domain was meshed with $4.6 \cdot 10^6$ fluid cells. The particle-to-cell size was $d_p/\Delta x_{BO} = 4.8 - 24$ (for cylinders) and $d_p/\Delta x_{BO} = 12$ (for spheres/cubes) CVs, which allows for an adequate representation of the particle shape.

2.2.2 Convective heat transfer fluid – particle

The rate of convective heat transfer, denoted as $S_{E,CV}$ [W], is expressed by the equation:

$$S_{E,CV} = \frac{1}{\varphi}\frac{k_{f,CV}}{L_{CV}}\left(T_{f,CV} - \bar{T}_{pf}\right)A_{CV} \tag{7}$$

φ is the ratio (A_P/A_{CFD}), where A_P is the actual particle surface area and A_{CFD} the enlarged particle area in CFD. L_{CV} is a charctersitic cell size, $T_{f,CV}$ is the fluid temperature in the cell, and $\bar{T}_{pf}$ represents the mean particle surface temperature associated with the cell. A_{CV} is the interfacial area in the cell. This source term S is also applied to the particle mesh as a boundary condition.

$$S_{pf} = \sum_{CV}^{CVs\in pf} \frac{S_{E,CV}}{N_{pf,CV}} \tag{8}$$

Whereby $N_{pf,CV}$ is the number of particle surfaces contained in the CV.

Please note that heat transfer through direct particle contact has been neglected, as convection, when present, dominates over contact heat transfer.

2.2.3 Radiative heat transfer

Radiative heat transfer between particle-particle and particle-wall is calculated with a Blocked-Off / Discrete-Ordinates-Model (BO/DO), described in more detail in [15]. This approach calculates the radiative transfer equations (RTE) on a cartesian grid, embedding the particle boundaries in the same manner as before. In its simplest form (no gas absorption), the RTEs are defined as:

$$\underline{\nabla}\cdot\left(I(\underline{s},\underline{r})\underline{s}\right) = \frac{E}{4\pi} \tag{9}$$

$I(\underline{s},\underline{r})$ is the radiative intensity at position $\underline{r}$ and for direction $\underline{s}$ and E is the emission due to the particle boundary. Particle surfaces are assumed to be gray and diffusive.

2.2.4 Pyrolysis Model

In this work, pyrolysis occurs in thermally thick particles, which means that particle internal transport must be resolved on a particle internal 3D mesh. The model used here is described in [11]. The model considers three components, which are reacting solid biomass (~80% of mass), solid char (~20% of mass) and gaseous volatiles (converted from biomass). Kinetic parameters (k, E_A) for conversion of

Copyright© Department of Fluid Mechanics, Budapest University of Technology and Economics and the Authors

biomass→volatiles are 168.4 s^{-1} / 51,965 J $(mol\ K)^{-1}$ and 13.2 s^{-1} / 45,960 J $(mol\ K)^{-1}$ for biomass→char. Gaseous volatiles have a fixed mass composition of 4.46/0.82/11.1/83.62% (CH_4/CO/H_2/CO_2). Solid conductivity and heat capacity of biomass and char were modelled with temperature dependent. Solid and gaseous components are in thermal equilibrium. Anisotropy is considered and (temperature dependent) thermal conductivity along the fibre direction was twice as high as across the fibre for all particles. Enthalpy of pyrolysis was not considered here, as it is neglectable small compared to the external heat added to the particle. The diffusion coefficient was assumed to be isotropic ($3 \cdot 10^{-3}$ $m^2 s^{-1}$). All particles contained no water, so a drying phase prior to pyrolysis did not occur.

3. DEM/CFD SIMULATION SETUP

3.1 Individual Particles, Simulation Domain, and Boundary Conditions

Three different model bodies are investigated in the numerical simulations: spheres, cubes, and cylinders (Figure 2). The dimensions of the model bodies were chosen such that all bodies have the same surface-to-volume ratio of 0.6 mm^{-1}. This corresponds to a radius of 5 mm for a sphere, an edge length of 10 mm for a cube, and a length and radius of 20 mm and 4 mm, respectively, for a cylinder (see Table 1). The particles are made of beechwood, for which an average (atro) density of 700 kg/m^3 was specified. Their initial temperature is 298 K.

The thermochemical conversion of the particles takes place in a cylindrical reactor flushed by hot nitrogen at T = 973 K and $\underline{u_f}$ = 0.14 m/s ($\dot{m}$=1.16 g/s). The walls of the reactor were at 973 K as well; thus, the bed is heated additionally by radiation. A slightly larger cylindrical tube (not depicted) is placed above the reactor into which the released volatiles enter and may combust (not investigated here). The packed beds were generated by allowing for particles to fall from above into the reactor until a bed height of 50 mm was reached.

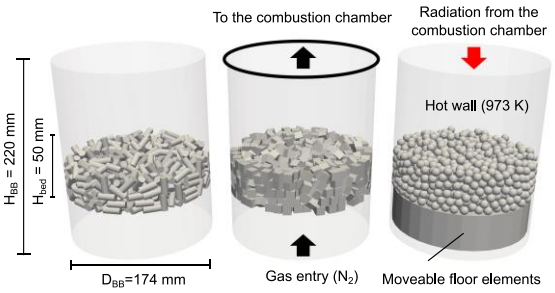

Figure 2. Pyrolysis reactor with movable base elements, stacked cylinders, cubes, spheres.

The bed was then mixed using movable floor elements, and more particles were added to restore the bed height to 50 mm. Due to the different volumes of the model bodies, this corresponds to different final number of particles and different bed porosities in the respective bed (left column). In the following, we refer the three packings simple as sphere, cube and cylinder bed, respectively.

4. RESULTS

4.1 Pyrolysis of single particles

Figure 3 shows the time evolution of the core temperature and the (dimensionless) particle mass for three (individual) particles of the respective shapes. Particles were placed into uniform radiation fields whose radiative intensities correspond to temperatures of T_{rad} = 700 C°, 800 C° and 900 °C. Convective heat transfer was not considered in these cases.

Table 1. Geometric properties of the three different particle shapes

Shape (N_P, ε_{bed})	Var. [mm]	A [10^{-4} m^2]	V [10^{-6} m^3]	m [10^{-4} kg]
Sphere (1278, 44%)	$r = 5$	3.14	0.52	3.2
Cylinder (636, 46%)	$r = 4$ $h = 20$	6.03	1.01	6.2
Cube (731, 39%)	$a, b, c = 10$	6.0	1.0	6.2

The core temperature rises faster with increasing T_{rad} and the thermochemical mass conversion (solid→gas) is completed earlier. It is noticeable that the core temperatures of the spheres and cylinders are very similar and increase faster than those of the cubes. For the cylinders, the distance between the shell surface and the core is the smallest (4 mm), which is why heat from the surface reaches the core faster than for the other two bodies. For spheres and cubes, the distance is 5 mm, whereby the distance from the surface to the core remains constant for the sphere but increases towards the corners for the cube. The heat flow in the cube is not exclusively in the direction of the core. Heat is also conducted in the direction of the corners/edges and is distributed there in the additional volume. Compared to the sphere, both the cylinder and the cube have about twice the surface area and about twice the volume and mass. More heat can therefore be exchanged over the surface of these two shapes, but more heat is required to heat the particles at the same time. After ~40 s, the

Copyright© Department of Fluid Mechanics, Budapest University of Technology and Economics and the Authors

heating rate of the particles at 900 °C slightly decreases. This is because heat conductivity increases with temperature and more heat is required to further increase particle temperature. For 500°C and 700°C, although heat conductivity also increases, it is not enough to be reflected in the mean temperature curve.

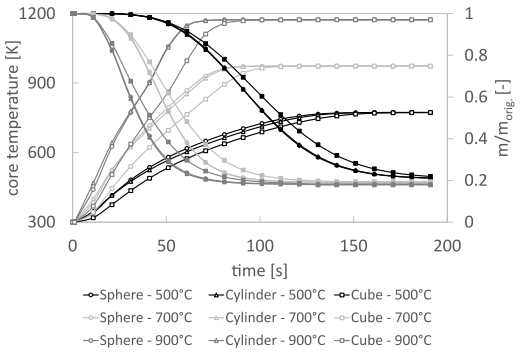

Figure 3. Core temperature and mass over time for the three particle shapes at 500 °C, 700 °C and 900 °C radiation temperature.

The mass conversion of solid biomass mainly depends on the temperature evolution within the particle and therefore, the mass evolution corresponds well to the core temperature evolution: Spheres and cylinders have almost identical mass evolution over time, whereas the mass of the cube decreases more slowly at the respective T_{rad}.

4.2 Total mass evolution within the bed

The temporal evolution of the (dimensionless) mass of the entire bed is presented in Figure 4. The sphere bed is converted the fastest, followed by the cylinder bed. The fixed cube bed is converted the slowest. This basically follows the trend that has already been observed for the individual particles, although the differences between the thermochemical conversion of the sphere and cylinder bed can be seen more clearly in the fixed bed.

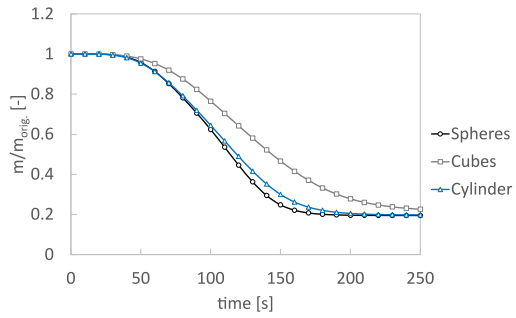

Figure 4. Dimensionless fixed bed mass of the sphere, cube and cylinder bed over time.

The complete conversion of biomass to char (approx. 20% by mass) takes place in around 180–250 seconds for spheres and cylinders, while for the cubes, pyrolysis is still not finally completed.

4.3 Flow field and convective heating within the packed bed

Snapshots of the fluid temperature field in the three packings as well as local velocity vectors are depicted slopes in Figure 5 in a cross-sectional view (t = 50 s). Based on the similar distribution and magnitude of the velocity vectors, it can be concluded that the flow within the sphere bed (top) is homogeneous, which can be attributed to its regular bulk morphology, i.e. homogeneously distributed void spaces / porosity.

The cube (middle) and cylinder (bottom) beds exhibit more complex flow conditions and larger local deviations. This is because the particles in the bed form more complex channel structures with larger statistical variation (heterogeneous porosity distribution).

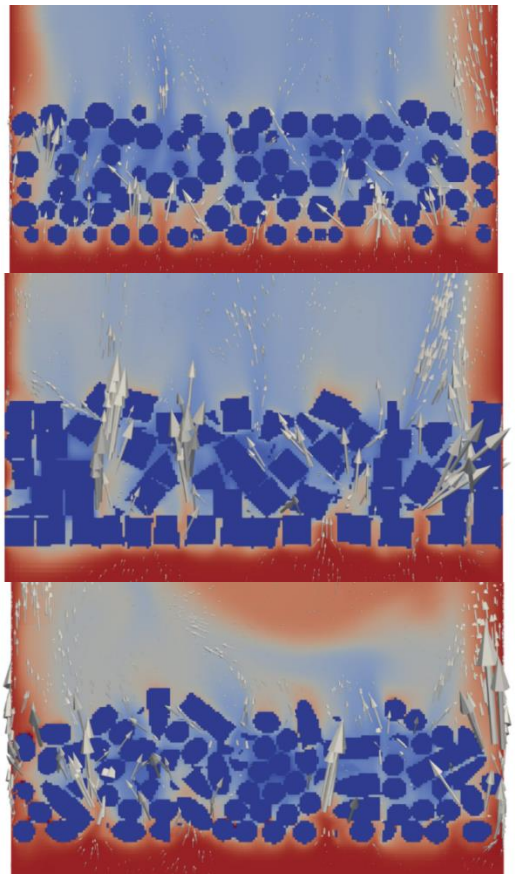

Figure 5. Cross-sectional snapshot of fluid temperature field in the three packings at t = 50 s. The arrows indicate magnitude and direction of the local fluid velocity.

This leads to locally constricted flow channels, which result in higher flow velocities (seen in the

Copyright© Department of Fluid Mechanics, Budapest University of Technology and Economics and the Authors

larger arrows), e.g. in the case of cylinders near the walls where the local porosity approaches very small values. However, there are also differences between the cube and cylinder bed. In the case of cubes, the flow is predominantly axial with cross flows being suppressed, particularly near the walls, as there the cubes tend to stack directly on top of one another. In the case of the cylinder bed, the velocity vectors within the bulk have a larger horizontal component, indicating enhanced cross-mixing.

The immediate effect of these flow conditions on the temperature profile is also observable in Fig. 5. The temperature front (red color) penetrates the sphere bed homogeneously in axial direction. However, for the cube and cylinder bed, the penetration is more strand-like, which is for example seen around the lowest particle layers. The narrow channels, constructed by the particles, allow for an effective but straightened penetration of hot nitrogen into the bed.

In the cylinder bed particles, radial penetration near the wall is more pronounced due to the aforementioned cross flow conditions. The sphere bed exhibits a slightly weaker penetration near the wall, as approximately only one particle layer is enveloped by the hot fluid at this point in time. Radial penetration in the cube bed is negligible, as the flow is predominanteley axial and radial components are effectively blocked by the stacked cube arrangement.

In summary, the sphere bed particles exhibits homogeneous heating, whereas the beds of cylinders and cubes experience more heterogeneous heating due to differences in convective heat transfer

4.4 Radiative heating

Initially, only the particles in the outermost bed layers, which are visible to the hot walls, are heated by radiation. However, as soon as the particles are hot enough, they also emit radiative heat and heat up other visible particles. The effect of radiation in the beds is described with Figure 6, depicting the particle surface temperatures. The cross section was cut in half, with the middle axis indicated by a dashed line on the left and the wall shown on the right.

Penetration of radiation into the bed differs for the three beds. In the sphere bed (left), radiation reaches only a short distance due to the tight packing of the spheres (ε = 44%), which effectively blocks radiation from penetrating deeper layers. The thight packing, in combination with the homogeneous packing structure, prevents what we call partial shadowing. Partial shadowing occurs when one particle is partially visually obstructed by its immediate neighbours so that only fractions of far range radiation reach the particles surface. This leads to non-uniform particle heating with locally larger temperatures at the particles „visible" surface and colder surface areas at the visually blocked surfaces. As partial shadowing does not occur for the sphere bed, the surface temperatures depict only minimal temeprature gradients.

In the cube bed (middle), the stacked cubes adjacent to the wall initially block most of the wall-emitted radiation, preventing significant penetration into the bulk material. This face-to-face stacking near the wall results in locally low porosity. Although the packing becomes looser deeper in the bed, the overall porosity remains low at 39%. As the wall-adjacent particles heat up and particle-to-particle radiative transfer becomes more significant, radiation begins to penetrate further into the bed. Despite the more heterogeneous structure compared to the sphere bed, partial shadowing effects remain limited due to the dense stacking of the cubes.

The cylinder bed (right) exhibits the largest porosity (46%). While it is only slightly larger than for the sphere bed, the cylinder form larger void spaces between them due to their high aspect ratio (h/r = 5), leading to the highest particle-particle visibility. Wall radiation can penetrate further inside the bulk right from the beginning. Furthermore, a competing behaviour between convection and radiation exists: Particles are already heated from a distance by radiation and then receive less thermal energy from the fluid flow, once its temperature front reaches the particles. In addition, partial shadowing plays a major role due to the large aspect ratio of the cylinders. Both effects contribute to temperature gradients across the cylinder surfaces, visible in the right side of Fig. 6

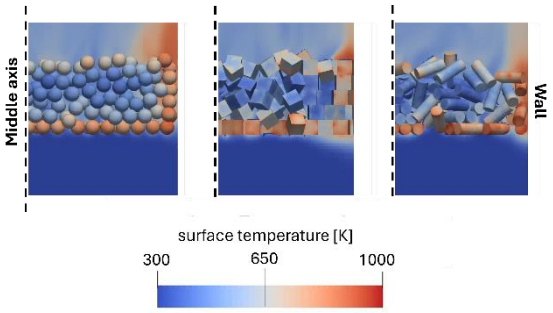

Figure 6. Comparison of particle surface temperatures.

4.5 Pyrolysis progress in the particle beds

Evolution of particle mass distribution is explained in conjunction with the concentration of CO_2 (as representative species for volatiles released) above the particle bed. Snapshots of the particle mass distribution at four different times (top to bottom) are shown in Figure 7 and CO_2 concentrations in the gas above the bed in Figure 8. After 50 s, particles in the outer layers of the beds have lost mass due to thermochemical conversion, induced by a) convective heat and b) radiative heat, both affecting the outer bed layers first. While differences in the mass distribution are not very distinct for the three

Copyright© Department of Fluid Mechanics, Budapest University of Technology and Economics and the Authors

beds at this specific time, the CO_2 concentrations above the beds clearly show that particles pyrolyze differently, depending on their shape and the local packing. The CO_2 concentrations are the highest near the wall in all cases, as particles there pyrolyze first. For the cylinder bed, some eddies are visible in the flow field above the bed while the flow through the sphere / cube bed is straightened and therefore, no eddies are present above the bed.

After 100 s, one can distinguish two zones in the sphere bed (Fig. 7, left). A core zone, with mostly un-pyrolyzed particles and layers of pyrolyzed particles around this zone. The boundary between these two zones is clearly identifiable. However, for the cylinder bed, (Fig. 7, middle), such a distinct boundary is barely visible, and for the cube bed, no distinct boundary is visible, indicating a more heterogeneous progression of pyrolysis. While the conversion progress for cylinders in the outer layers is relatively uniform (m/m_0 = 0.2–0.3), those located in the core exhibit significantly greater variability in their conversion rates. Cubes in the inner and outer layers show a quite heterogeneous conversion progress, ranging from 0.3 to 1.

From Fig. 8 at 100 s, one can deduce that pyrolysis is now occurring in the whole particle bed and not just near the wall, as CO_2 covers the whole volume above the beds. CO_2 is distributed quite evenly above the sphere bed and the profile appears symmetric around the middle axis, indicating that thermal conversion of the solid material and subsequent release of gaseous volatiles occurs in a spatial homogeneous manner. Cubes near the wall still pyrolyze and, therefore, higher CO_2 concentrations are visible. Furthermore, elevated CO_2 concentrations are observed below the bed. This is attributed to the cubes obstructing the flow paths, causing minor backflow that also carries CO_2 in the reverse direction. CO_2 concentrations above and inside the cylinder bed appear most heterogeneous. This is due to: (a) the uneven progression of pyrolysis among the particles (see Fig. 7), and (b) the complex flow conditions within the cylinder bed resulting from irregular flow pathing.

At 150 seconds (Fig. 7), the appearance of the pyrolysis zones remain largely consistent with those observed at 100 seconds, i.e., symmetrical in the sphere bed, indicating homogeneous conversion, and asymmetrical in the beds of cubes and cylinders, reflecting heterogeneous conversion. The CO_2 concentrations at 150 s are quite different (Fig. 8) for the three beds. The sphere bed exhibits a candle flame-shaped distribution of CO_2. Particles in the outer layers are completely pyrolyzed and already released all volatiles. Pyrolysis in the cube bed is still ongoing in the whole bed and, therefore, the whole volume above the bed contains CO_2. Like the spheres, cylinders in the outer bed layers are already completely pyrolyzed and only the cylinder in the core region release volatiles. Again, due to the heterogeneous conversion and the flow pathing, the CO_2 distribution is spatially very heterogeneous.

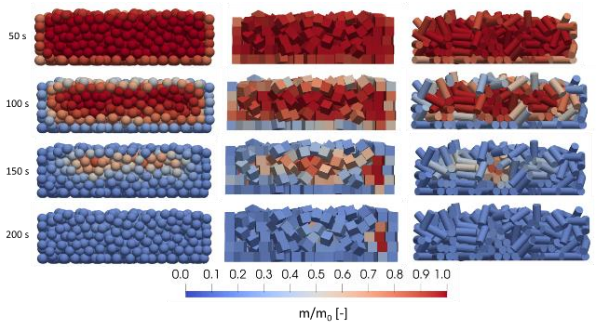

Figure 7. Cross-section of the three particle packings and colored representation of the dimensionless particle mass (t = 50 s, 100 s, 150 s and 200 s, from top to bottom).

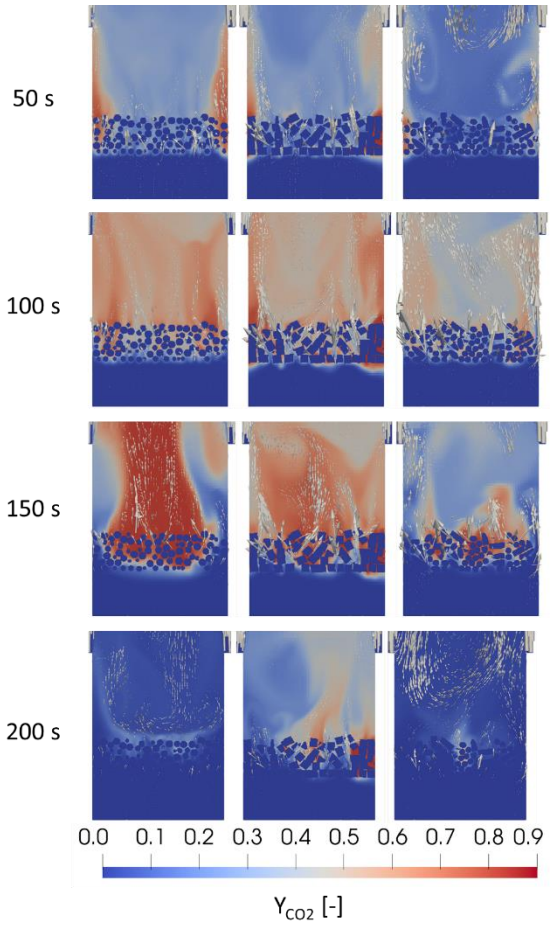

Figure 8. CO_2 mass fraction (cell values) in the gas phase in and above the bed (t = 50 s, 100 s, 150 s and 200 s, top to bottom) for spheres, cubes and cylinders, respectively (from left to right).

After 200 s, thermal conversion is largely completed. The sphere bed is nearly completely pyrolyzed and only little CO_2 remains in the gas phase. In contrast, the cube bed exhibits the slowest

Copyright© Department of Fluid Mechanics, Budapest University of Technology and Economics and the Authors

conversion, with some particles in the core region still undergoing pyrolysis. The cylinder bed is also mostly converted, and similar to the sphere bed, only low concentrations of CO_2 remain.

5. SUMMARY

In this work, DEM/CFD simulations of the pyrolysis of particle beds containing thermally thick beechwood particles of three different shapes were conducted. Spheres, cubes and cylinders constituted the beds. The differences in the pyrolysis behaviour of the solid particles and in volatile gas concentrations were investigated.

The total conversion of the bed is fastest for the spheres, followed by the cylinders and then the cubes. Total bed conversion over time for spheres and cylinders is similar.

For the investigated shapes, local conversion of solid particles is spatially very different, as are the flow conditions in and above the beds.

Generally, the pyrolysis zone, where particles mainly undergo conversion, is spatially very homogeneous for the sphere bed but heterogeneous for the other two beds. This is attributed to the flow field and the radiative conditions within the bed, which depend on the packing structure. All beds pyrolyze from their outer layers towards their core. However, the pyrolysis front traveling into the bed is symmetric for the sphere bed with a distinct pyrolysis reaction front detectable. This is not the case for the beds of the other two bodies. Accordingly, volatiles in the sphere bed are distributed evenly in the gas phase, in and above the bed over the whole process duration. The beds of cubical and cylindrical particles exhibit locally larger volatile concentrations, depending on the local conversion progress and the flow conditions.

This paper demonstrates that DEM/CFD simulations representing particles as spheres—a common simplification used to reduce computational cost—may be highly misleading when the actual particles are non-spherical.

ACKNOWLEDGEMENTS

This work has been funded by the Deutsche Forschungsgemeinschaft (DFG, German Research Foundation) – Project-ID 422037413 – TRR 287.

REFERENCES

[1] A. H. Mahmoudi, F. Hoffmann, and B. Peters, "Detailed numerical modeling of pyrolysis in a heterogeneous packed bed using XDEM," *Journal of Analytical and Applied Pyrolysis*, vol. 106, pp. 9–20, 2014.

[2] X. Gao, J. Yu, L. Lu, and W. A. Rogers, "Coupling particle scale model and SuperDEM-CFD for multiscale simulation of biomass pyrolysis in a packed bed pyrolyzer," *AIChE Journal*, vol. 67, no. 4, p. 127654, 2021.

[3] J. Wiese, F. Wissing, D. Höhner, S. Wirtz, V. Scherer, U. Ley, and H. M. Behr, "DEM/CFD modeling of the fuel conversion in a pellet stove," *Fuel Processing Technology*, vol. 152, no. 2, pp. 223–239, 2016.

[4] F. Buss, S. Wirtz, and V. Scherer, "Simulation of a reacting agitated bed of straw pellets by a resolved coupled DEM/CFD method using a blocked-off approach," *International Journal of Thermal Sciences*, vol. 152, p. 106332, 2020.

[5] R. Mittal and G. Iaccarino, "Immersed Boundary Methods," *Annu. Rev. Fluid Mech.*, vol. 37, no. 1, pp. 239–261, 2005.

[6] S. Das, N. G. Deen, and J. Kuipers, "Direct numerical simulation for flow and heat transfer through random open-cell solid foams: Development of an IBM based CFD model," *Catalysis Today*, vol. 273, no. 1, pp. 140–150, 2016.

[7] S. Das, N. G. Deen, and J. Kuipers, "A DNS study of flow and heat transfer through slender fixed-bed reactors randomly packed with spherical particles," *Chemical Engineering Science*, vol. 160, no. 15, pp. 1–19, 2017.

[8] C. Gorges, M. Brömmer, C. Velten, S. Wirtz, E. I. Mahiques, V. Scherer, K. Zähringer, and B. van Wachem, "Comparing two IBM implementations for the simulation of uniform packed beds," *Particuology*, vol. 86, pp. 1–12, 2024.

[9] V. Chéron, F. Evrard, and B. van Wachem, "A hybrid immersed boundary method for dense particle-laden flows," *Computers & Fluids*, vol. 259, p. 105892, 2023.

[10] E. Illana Mahiques, M. Brömmer, S. Wirtz, and V. Scherer, "Locally Resolved Simulation of Gas Mixing and Combustion Inside Static and Moving Particle Assemblies," *Chem Eng & Technol*, vol. 46, no. 7, pp. 1362–1372, 2023.

[11] B. Jaeger, E. Illana Mahiques, S. Wirtz, and V. Scherer, "Pyrolysis of Spherical Wood Particles in a Packed Bed – Comparison between Resolved and Unresolved Discrete Element Method/Computational Fluid Dynamics," *Chem Eng & Technol*, vol. 46, no. 10, pp. 2120–2132, 2023.

[12] OpenFOAM wiki, *FireFoam.* [Online]. Available: https://openfoamwiki.net/index.php/FireFoam (accessed: Aug. 22 2023).

[13] M. Brömmer, M. Scharnowski, E. Illana Mahiques, S. Wirtz, and V. Scherer, "Investigating the inflow into a granular bed using a locally resolved method," *Particuology*, vol. 85, no. 1, pp. 89–101, 2024.

[14] B. Jaeger, M. Tyslik, S. Wirtz, and M. Schiemann, "Investigation of the radiative heating of cubic particles with DEM/CFD and the BO/DO approach," *Powder Technology*, vol. 403, no. 6, p. 117424, 2022.

Copyright© Department of Fluid Mechanics, Budapest University of Technology and Economics and the Authors